iJRASET
International Journal For Research in Applied Science and Engineering Technology

INTERNATIONAL JOURNAL FOR RESEARCH

IN APPLIED SCIENCE & ENGINEERING TECHNOLOGY

Volume: 10 **Issue:** XI **Month of publication:** November 2022

DOI: https://doi.org/10.22214/ijraset.2022.47164

www.ijraset.com

Call: 08813907089 | E-mail ID: ijraset@gmail.com

International Journal for Research in Applied Science & Engineering Technology (IJRASET)
ISSN: 2321-9653; IC Value: 45.98; SJ Impact Factor: 7.538
Volume 10 Issue XI Nov 2022- Available at www.ijraset.com

An Advanced Electro-thermal Averaged Model of PWM Switch Cell

Slim ABID[1], Houssem Ben Arabia[2], Nouredine Ferchichi[3], Zuhair Alaas[4]
[1, 2]*Jazan University Saudi Arabia*
[1, 2, 3, 4]*National Engineering School of Sfax, Power Electronic Group BP 1173, 3038 Sfax, Tunisia*

Abstract: ***In this paper, a new electro-thermal averaged model of PWM switching cell is presented. The main advantages of the proposed averaged model are that takes into account the nonlinear effects of semiconductor devices their electrical inertia and self-heating. It is useful in determining the device's heat generation, junction temperature as well cooling performance of the connected heat sinks. The proposed electro-thermal model is general and can be applied to different DC/DC and DC/AC converters. The accuracy of the model in a simulation of the temperature dependence is verified through SABER simulation for the Buck converter and one-leg inverter.***

Keywords: Electro-thermal averaged model, the nonlinear effects of semiconductor devices, self-heating, 1D thermal model, junction temperature.

I. INTRODUCTION

In recent years, power semiconductor devices, especially IGBT and MOSFET, are widely used in a lot of industrial applications, such as power suppliers, motor drives, power systems, and consumer electronics. Due to the demand for high power density, the losses of power devices and the resulting thermal problems are more and more emphasized, because the high temperature would result in the failure of power devices and the surrounding components. They are the key factors that could influence the whole system's reliability and efficiency.[1-2]

To determine the losses in the semiconductor devices and to evaluate the cooling performance of the connected heat sinks, an accurate approach is to simulate a circuit by using a physically-based device model [3–5]. However, due to the complicated physical switching process, and the very fast transient period, this study requires very small simulation time steps (in the order of nanoseconds), which result in an unacceptably large CPU time and memory storage; for a multi-device power electronics systems and real-time simulation, the problem is even more intractable [. At the other end of the scale, it is common to use device datasheets, provided by manufacturers, to estimate losses [9]. This method is simple but can be very inaccurate. It is clear that a method is needed which is fast and yet accurate at the system level. To reduce simulations time, we have proposed in [10-11] an average PWM-Switch model including semiconductor device non-linearity. The effects of the driving signals characteristics, the Dc loop inductance, the switching power losses, and the I-V characteristic are taken into account. Unfortunately, this model is an electrical model that neglects the effect of self-heating of semiconductor devices. In the present paper, we have developed a non-ideal averaged model of the PWM-switch which takes into account the evolution of the junction temperature. The developed model is useful for determining the device's heat generation, junction temperature as well cooling performance of the connected heat sinks. The model provides accurate results without the need for an unreasonably small time step. The approach taken consists of two stages. First, the electrical averaged model is obtained by mathematical derivation from the known idealized switching characteristics of the active device switching characteristics. The electrical simulationof the averaged model gives the required electrical characteristics such as the effective voltage and current for power loss calculation. Then, the average power loss over each simulation time step has been mathematically calculated using the defined device characteristics in the look-up tables. After, by feeding this average power loss into a compact thermal network, the junction temperatures of devices are calculated. Because the device losses are functions of temperature, the computed device temperature is then used to change the parameters of the switch loss model for the next time step. This method is suitable for a long real-time thermal simulation for DC-DC and DC-AC power devices with arbitrary load operation. Throughout this paper, the simulation time step is set equal to the PWM switching period. This paper develops a complete average electrothermal model of the PWM switch. And experimental investigations have been performed in order to identify the different model parameters as a function of the load direct current and the applied junction temperature. The thermal parameters of each device are performed too. Finally, the accuracy of the advanced dynamic electrothermal averaged model has been studied in the case of DC/DC and DC/AC converters. The comparison between the obtained results with those obtained by the electrical averaged model and SABER simulation is performed.

II. DERIVING THE NON-IDEAL AVERAGED MODEL OF THE PWM-SWITCH

The average model of a converter is a simplified representation of the converter in quasi-cyclic operation that pictures the energy transformation without using explicitly any switching function [12]. The studied PWM-switch structure is given in Figure (1.a), it has two basic switching cells (P-cell and N-cell). Each cell consists of one controlled switch and one diode. The four classical DC/DC converters (Buck, Boost, Buck-Boost, Cuk) can be easily decomposed into a P-cell and N-cell base circuit. In addition, the parallel combination of the N-cell and P-cell provides a bi-directional current flow switching cell. Therefore, bi-directional DC/DC converters and all inverters can be constructed.[11]

The voltage source Ve can be an input or output DC voltage source according to the converter structure. The stray DC loop inductance is represented by an inductor L_{st}.

Depending on the sign of the load current I_L, only two devices (one switch and one diode) operate.

The proposed averaged model of the PWM-switch is presented in Figure1.b. This model contains a controlled voltage source (V_1) and a controlled current source (I_1). The PWM-switch is the only nonlinear element that is supposed to be responsible for the non-linear behavior of the converter.

The permutation of the two sources' positions is possible. In the proposed configuration, the current through the voltage source and voltage across the current source can be deduced.

Considering T_s as the switching period of the controlled switches and (d) the duty ratio which is the ratio of the on-time value (T_{on}) of the upper controlled switch (T_1) and the switching period T_s.

In Figure (1.b), the current source (I_1) and the voltage source (V_1) are given by

$$V_1 = < U_{as} > \quad (1) \qquad I_1 = < i_{e2} > \quad (2)$$

Where $<U_{as}>$ and $<i_{e2}>$ are the time averaged values of the instantaneous terminal waveforms $U_{as}(t)$ and $i_{e2}(t)$ respectively over one cycle Ts.

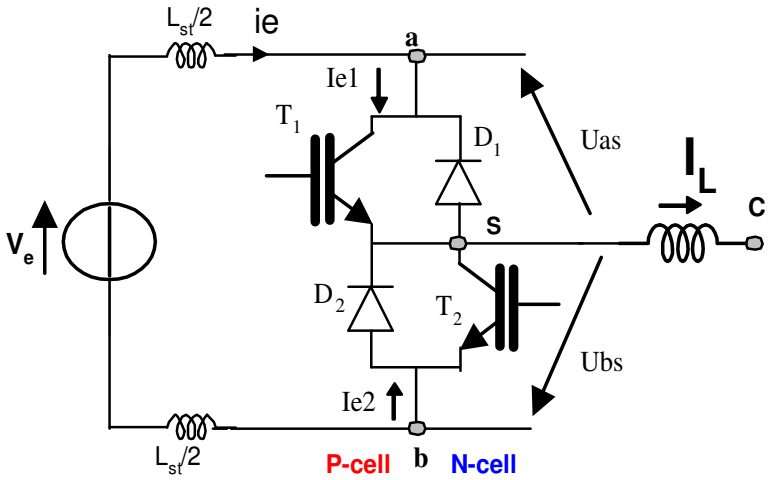

(a)

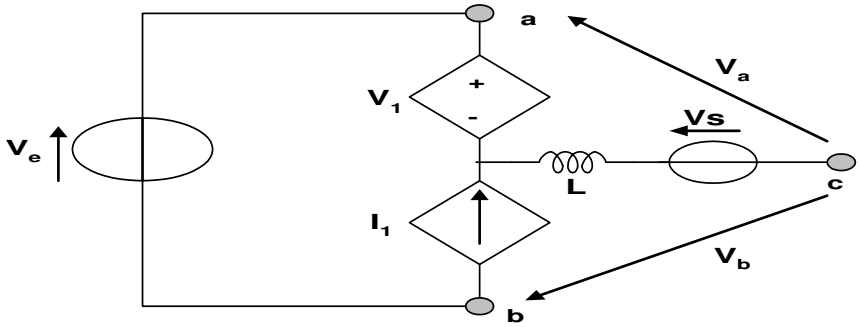

(b)

Fig.1. (a) The PWM-switch, (b) The proposed equivalent circuit of the PWM-Switch averaged model.

Figure 2 pictures the adopted switching characteristics of the IGBT (T_1) ($U_{as}(t)$, $i_{e1}(t)$) and the free-wheeling diodes D_2($U_{bs}(t)$, $i_{e2}(t)$) during Ts. e_{g1} and e_{g2} are the driving signals of the controlled components T_1 and T_2, respectively. We notice that Dc loop inductance, the reverse recovery phenomena, and the dead time δ between the two driving signals are taken into account. Figure 2 shows the case when $i_L(t)$ is positive, so only the controlled components T_1 and the diode D_2operate.

We notice that the load current I_L is considered constant and equal to the average value of the real current $i_L(t)$ in the load over the switching period Ts.

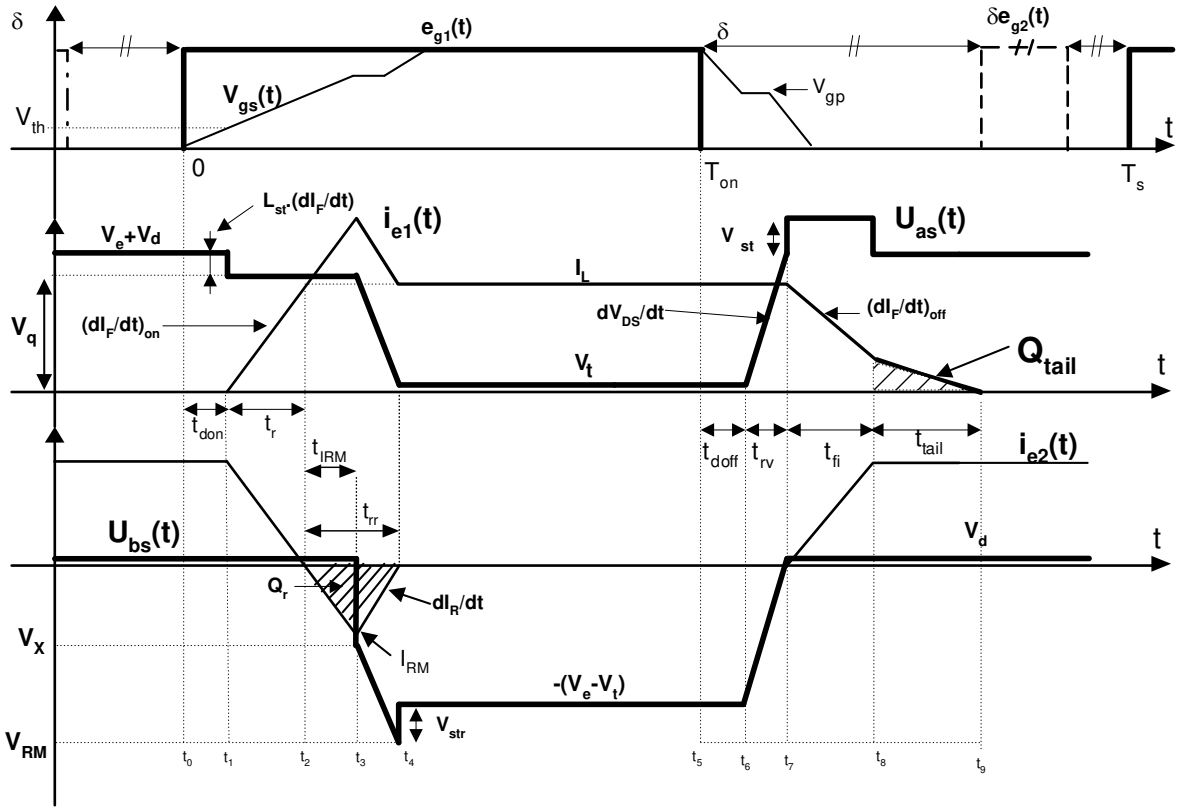

Fig.2. The adopted switching characteristics of the controlled and the diode devices in the PWM-switch

The averaged values of the voltage across the device of the voltage source V_1 and current I_1 are obtained by integrating the voltage and the current evolutions shown in Figure 2 over one cycle Ts. The parameter δ is the dead-time fixed by the user to eliminate the simultaneous conduction of the two controlled devices of the bidirectional PWM-switch.

The averaged dissipated power P_D in the different power devices is obtained by integrating the product of current and voltage evolutions, shown in Figure 2, over the switching period Ts.

$$P_D = \frac{1}{T_s}\int_0^{T_s} V(t)I(t)dt \qquad (3)$$

So,

$$P_{IGBT} = \frac{(I_L V_t)}{Ts}(d.Ts - t_{don} - t_r - t_{rr} + t_{doff}) + \left(\frac{(V_b - E - V_d)}{3Ts} + \frac{(E+V_d)}{2Ts}\right)(I_L + I_{RM})(t_r + t_{IRM}) + \left(\left(\frac{(V_b - V_t)}{3Ts} - \frac{V_b}{2Ts}\right)I_{RM}\right.$$

$$\left. + \left(\frac{(V_t - V_b)}{2Ts} + \frac{V_b}{Ts}\right)(I_{RM} + I_L)\right)(t_{rr} - t_{IRM}) + \frac{(E+V_d - V_t)}{2Ts} I_L t_{rv} + \frac{Vt}{Ts} I_L t_{rv} + \frac{(E+V_d+V_L)}{2Ts}(I_L + I_{tail}.X)t_{fi}$$

$$+ \frac{(E+V_d)}{2Ts} I_{tail}.X.t_{tail}$$

and

$$P_{DIODE}=\frac{I_L V_d}{Ts}(Ts-d.Ts+t_{don}-t_{doff}-t_{fi}-t_{rv}+t_{don})+\frac{I_{RM}}{2Ts}(V_L+V_{L1}-V_d)(t_{rr}-t_{irm})+\frac{I_{RM}}{6Ts}(V_b-V_t)(t_{rr}-t_{irm})+$$
$$\frac{I_L V_d}{2Ts}t_{fi}-\frac{I_{RM}}{2Ts}V_d t_{irm}$$

Where

$$X=\begin{cases}0 & \text{for MOSFET}\\ 1 & \text{for IGBT}\end{cases}$$

These switching delay times can either be measured or predicted using advanced compact models, but must be produced using the typical operating environment of the converter load and parasitic elements, which includes a fixed dc-link voltage. These results are then stored in a look-up table which effectively represents the pre-characterized device behavior.

III. ELECTROTHERMAL COUPLING SIMULATION

Figure 3 shows a diagram of the electrothermal simulation technique for power converters. In the proposed model, the power converter consists of a coupling between the electrical averaged model and the thermal model as shown in figure 3..

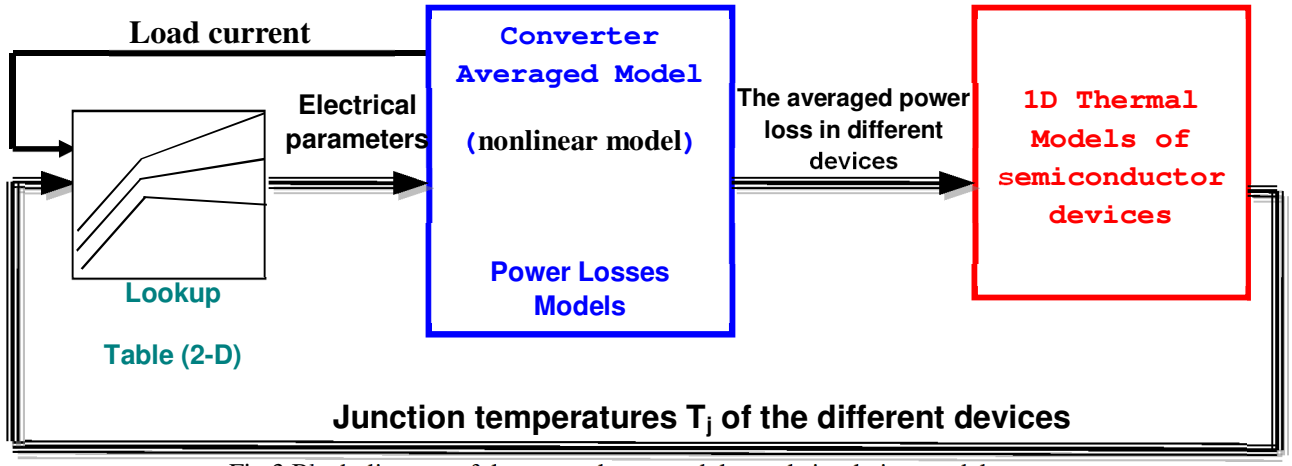

Fig.3 Block diagram of the power losses and thermal simulation model

The averaged model, where electrical characteristics of MOSFET or IGBT and diodes are defined, is coupled to the thermal model. The averaged values of the different devices' power losses are applied to the thermal models, in which the thermal characteristics of each device are defined. Then, the averaged device temperature is calculated by the thermal model. The electrical model parameters vary as a function of the devices junction temperature evolution and load current magnitude. This coupling is performed using the look-up table method in Simulink/Matlab environment.

The used semiconductor devices are the IGBT IRGBC20U (14A, 400V) and the diode BYT12P600 (15A, 600V). Their thermal models are described in detail in the next section.

IV. THERMAL NETWORK MODELS

The thermal models used in this paper are intended for analyzing the electrothermal performance of the power-electronic circuit. The junction temperature of each converter device is an important physical parameter influencing the device's electrical behavior.

Because most of semiconductor device models are implemented in circuit simulators, thermal circuit networks are the practical models for electrothermal simulations. The literature proposes some approaches to construct thermal networks equivalent to a discretization of the heat equation [14].

In the case of a vertical power device, where the thickness of the die L is small compared to other dimensions, it is commonly considered that heat is generated at the top surface of silicon and flows uniformly along the x-axes (perpendicular to the silicon surface A_s).

So the top surface is considered to be a geometrical boundary of the device at x=0,where the input power P_{in} (t) is assumed to be uniformly dissipated. The lower surface of the die (at $x=L_s$) is considered to be the cooling boundary, where the temperature is assumed to be equal to the input temperature $T_{in}(t)$. In this study, convection and radiation are assumed to be negligible. 1D heat flow may be considered for different device layers.

$$\rho c \frac{\partial T(x,T)}{\partial x} = K \frac{\partial^2 T(x,t)}{\partial x^2} \quad (4)$$

With boundary conditions

$$A.K \frac{\partial T}{\partial x}\Big|_{x=0} = -P(t)$$

and

$$T(t, x = L) = Ta$$

Thermal conductivity K is assumed to be constant equal to K_0 = 1.548 °C/W for the silicon. Studies in [12] have shown the advantage of the finite element method compared to the finite difference element method. The Finite Element Method (FEM) is based on a variational approximation of the heat equation.

The approximated solution of equation (4) is given by

$$\tilde{T}(x,t) = \sum_{i=1}^{n} \xi_i(t) W_i(x) \quad (5)$$

Where $W_i(x)$ are the decomposition functions and $x_i(t)$are the coordinates of the temperature approximation in the functional space basis formed by the decomposition functions. When a classical choice of a linear piecewise for the decomposition function $W_i(x)$ is done, the 1D thermal model can be represented by the equivalent circuit shown in figure 4.These thermal models are easy to implement in circuit simulators.

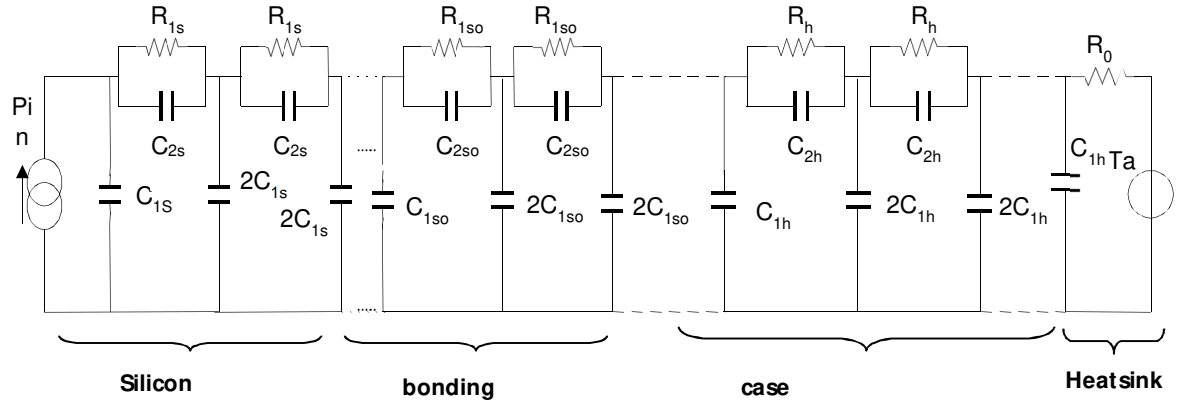

Fig.4. Equivalent thermal network of a semiconductor device and heat sink

For the silicon layer, for example, the network components are:

$$C_{1s} = \frac{\rho c A_s L_s}{2(n-1)},\ C_{2s} = -\frac{\rho c A_s L_s}{6(n-1)} \text{ and } R_{1s} = \frac{L_s}{(n-1)K.A_s}$$

h is the discretization step, ρ_s is the silicon mass density, c_s is the silicon specific heat,

Although some manufactures provide the values of R_{th} and C_{th} (junction to case thermal resistance and thermal capacitor) values in their device specification sheets. The information required to obtain thermal network parameters is commonly given in the form of a single-pulse junction to case transient thermal impedance (Zth-jc).

To identify the geometrical parameters of the different devices die, the adopted technique consists of using the transient thermal impedance given by manufacturer data sheets [15].

The estimation of the effective surface A and length L is performed by an identification procedure to research the optimal parameters corresponding to the accurate evolution of the temperature response given by the thermal model compared to the temperature evolution deduced from the transient impedance curves. So, the effective Area A and the effective length L of the different dies of the IRGBC20U and the BYT12P600 are shown in Table I.

Figure 5 and Figure 6 show the thermal impedance curves obtained by simulations (6 nodes model for silicon die and 2 nodes model for bonding and case dies) and from the manufacturer data sheets. As can be seen from Figure 5 and Figure 6, the Zth-jc curves obtained from the fitted thermal models show a good agreement with the corresponding data sheet curves.

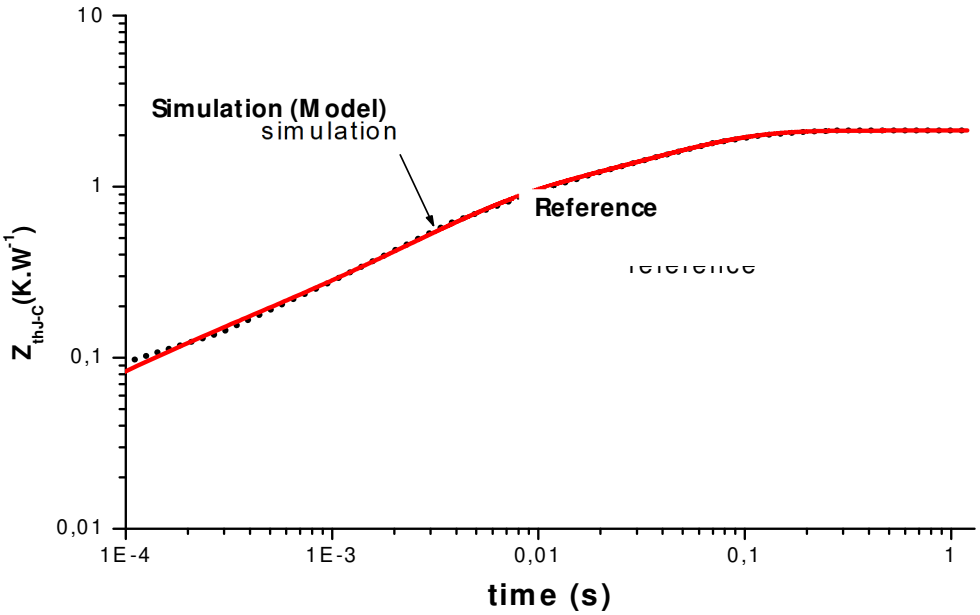

Fig.5. Comparison between the transient thermal impedance Zth-jc curves (IRGBC20U) obtained with simulation and from data sheet manufactures (reference)

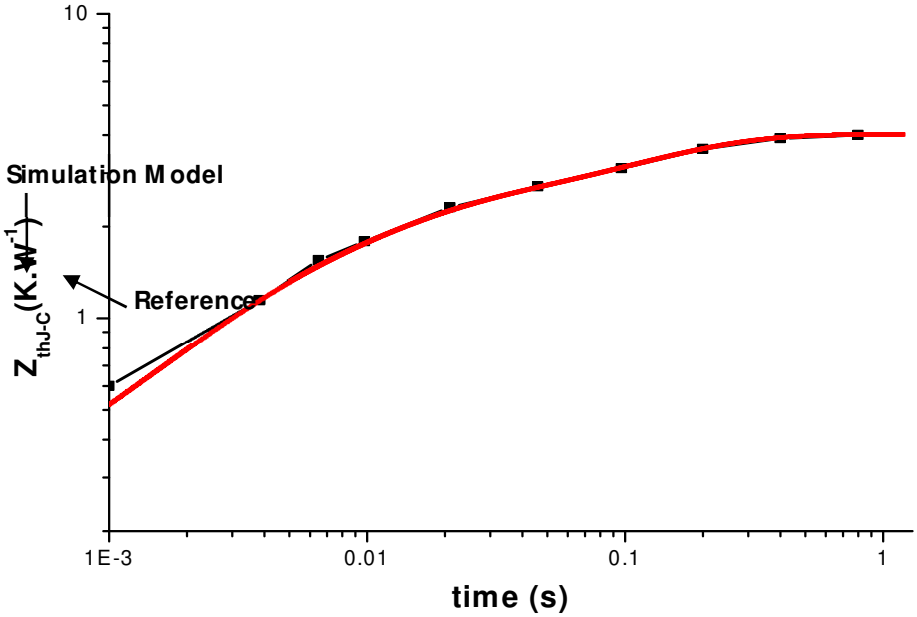

Fig.6. Comparison between the transient thermal impedance Zth-jc curves (BYT12P600) obtained with simulation and from data sheet manufactures (reference)

TABLE I
EFFECTIVE GEOMETRICAL PARAMETERS OF THE IGBT IRGBC20U AND BYT12P600

	K w/ mK	ρc J/km^3	S mm^2 IRGBC20U	Lm m	S mm^2 BYT12P600	Lmm
Silicon	134	1.7*10^6	8.4	380	4.8	300
Die bonding	35	1.3*10^6	8.4	100	4.8	100
Case	143	3.5*10^6	9.8	1600	5	2010

The thermal models are implemented in the circuit simulator SABER and in the Matlab toolbox (Simulink) simulator in order to couple thermal models to electrical models.

V. ESTIMATION OF THE PARAMETERS OF THE NONLINEAR ELECTROTHERMAL AVERAGED MODEL

The parameters of the averaged model of the bidirectional switching cell are: The static characteristics of the power devices, and the dynamic parameters. For a given power converter topology and command circuit characteristics, the user needs the evolutions of the adopted switching characteristics parameters (figure 2) as a function of the load current and the junction temperature.

A. Static Parameters Extraction

The steady-state losses in the diode and the IGBT are determined by the device saturation voltage and the device current. Therefore, the on-state voltage under different temperatures should be measured with a curve tracer (Figure 7). A hot air furnace is used to control the temperature of the devices under test. The measurement procedure of a static « on-state » is quite classical, so it is not discussed here. The only precaution is to limit the device under test self-heating.

Fig. 7. Curve tracer

Forward on-state voltage of the different components can be approximated by a linear characteristic given by :

$V = V_0 + R_{on}I$ (6)

Where: V_0 is the threshold value of the voltage across the device (Diode_Model or IGBT) and R_{on} is the equivalent resistance which defines the voltage across the device at the rated current (MOSFET, IGBT or Diode Model).

The dependence of $R_{on}$and $V_0$of the IRGBC20U and BYTP600 as a function of the junction temperature are shown respectively in Figure 8 and Figure 9.

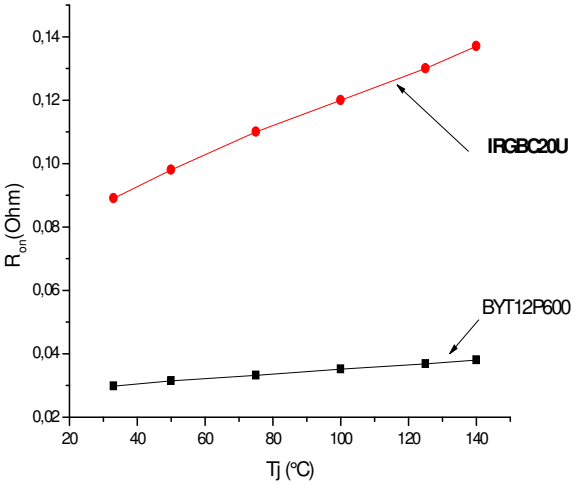

Fig.8. Experimental evolution of the on state resistance R_{on} of IRGBC20U and BYT12P600 versus the junction temperature Tj

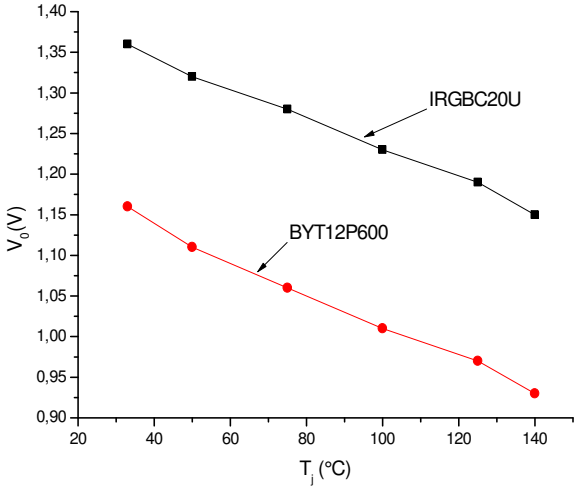

Fig.9. Experimental evolution of the threshold voltage V_0 of IRGBC20U and BYT12P600 versus the junction temperature Tj

The last curves can be approximated by a linear functions given by:

$$R_{on-IGBT} = 0.0786 + 4.0210^{-4}.T \text{ and } R_{on-diode} = 10^{-5}T + 0.025 \quad (7)$$

$$V_{0-diode} = -0.002T + 1.22 \text{ and } V_{0-IGBT} = 1.407 - 1.7310^{-3}T \quad (8)$$

V.2. Dynamic Parameters Extraction: For a given power converter topology and command circuit characteristics, the user need the evolutions of the adopted switching characteristics parameters (Figure.2) as a function of the load current and the junction temperature.

Figure 10 shows, the used circuit for dynamic parameters identification. The insulated gate bipolar IGBT (IRGPH40F) is used to avoid the self-heating of the diode and the IGBT under test, by deriving the current source I_F through another path most of the time. The inductors L_1 and L_Q (Figure 10) act as current sources during the (IRGPH40F) and (IRGBC20U) switching phases, respectively. Inductor L_1 is a large iron inductor and L_Q is an inductor that features high-frequency ratings. The IGBT (IRGPH40F) enables support of the conduction most of the time (Figure 11). The (IRGBC20U) is turned on before the (IRGPH40F) is turned off.

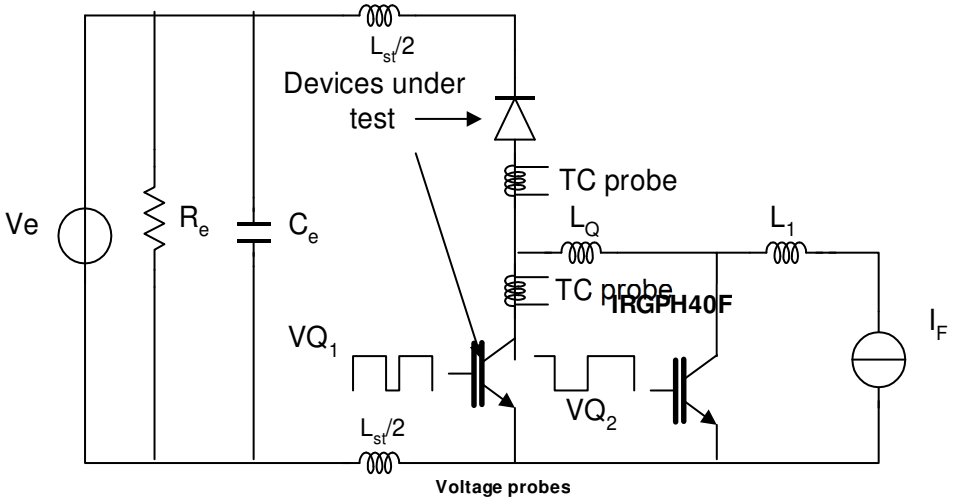

(a)

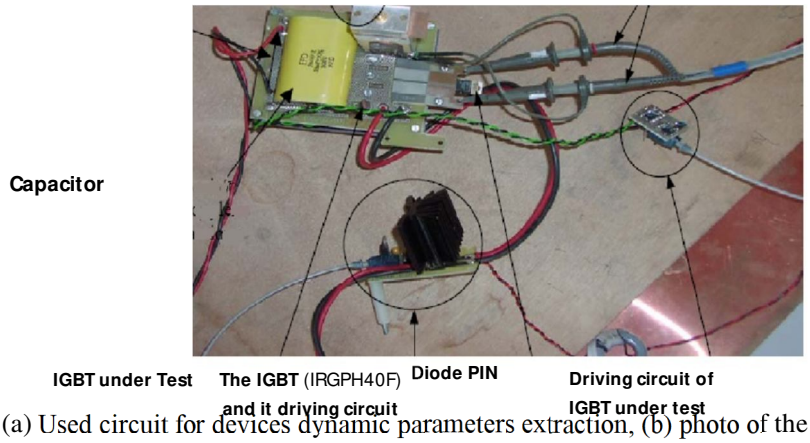

Fig.10. (a) Used circuit for devices dynamic parameters extraction, (b) photo of the used experimental circuit.

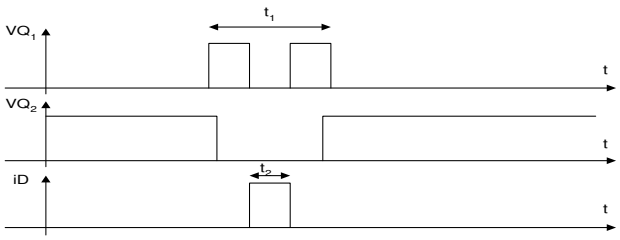

Fig.11. Typical driven signal and idealized diode current waveforms t2 the conduction time of the diode (2us<t2<10us), (t1-t2) the conduction time of the IGBT (4us<t1-t2 <20us)

The current flowing the semiconductor switch are measured with a TC probes (LESiR) of 200-MHz bandwidth. The voltage drop across the diode is obtained by computing the difference between the anode and cathode voltage values obtained by a 500 MHz voltage probes (Tek P139A). The voltage drop across the controlled device is obtained by the voltage probe placed at the anode diode pin. The measured waveforms i(t) and v(t) are obtained with an oscilloscope (Tek TDS744A of 500-MHz).

*V.2.1. Reverse maximum Current (I_{RM}) and the reverse recovery time (t_{rr}):*Under different conditions of state current (2A, 4A, 8A and 10A), and in an operating temperature range of 27°C to 140°C, the reverse-recovery phenomena occurring during diode turn-off are measured. Figure 12 and Figure 13 gives respectively the evolution of the maximum reverse current I_{RM} and the reverse recovery time t_{rr} of the BYT12P600 as a function of the load current magnitude and junction temperatures.

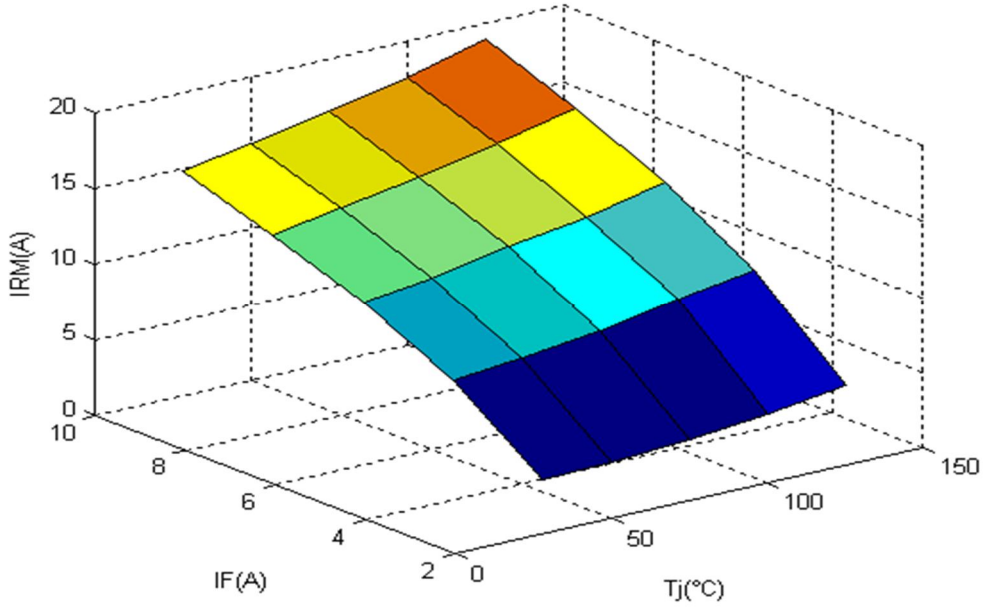

Fig.12. Look-up table, the maximal reverse recovery current IRM of the diode BYT12P600

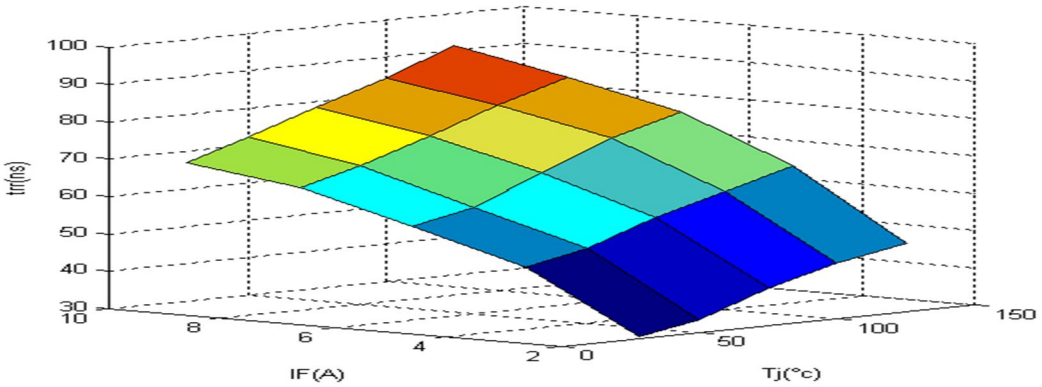

Fig.13. Look-up table, the reverse recovery time trr of the diode BYT12P600

The time t_{IRM} is given by :

$$t_{IRM} = \frac{I_{RM}}{\frac{dI_{IGBTon}}{dt}}$$

$\frac{dI_{IGBTon}}{dt}$is the slope rate of the current in the IGBT during turn on.

V.2.2. The current turn-on delay time (t_{don}) and the voltage turn-off delay time (t_{doff}):t_{don} and t_{doff} are the delay times of switching-on and switching-off of the IGBT respectively. These times can be calculated with the formulas [16]:

$$t_{don} = R_G C_{iss} Ln\left(\frac{1}{1-\frac{V_{th}}{e_g}}\right) \quad (9)$$

$$t_{doff} = R_G C_{iss} Ln\left(\frac{e_g}{V_{GP}}\right) \quad (10)$$

The V_{GP} voltage is given by [16]:$V_{GP} = V_{th}(T_j) + \frac{I_F}{g_{fs}}$

Where V_{th} designates the transistor threshold voltage, C_{iss} the input capacity, R_G the gate resistance, g_{fs} the transconductance and $e_g$the gate voltage supply.

The threshold voltage is the gate voltage at which the IGBT turns on and collector current begins to flow. IGBTs have a negative temperature coefficient for the threshold voltage as seen in Figure 14. The threshold voltage decrease when temperature increases. The increase in temperature leads to decrease in the band-gap of the silicon, which reduces the threshold voltage. It is therefore easier to turn-on the IGBT at higher ambient temperatures.

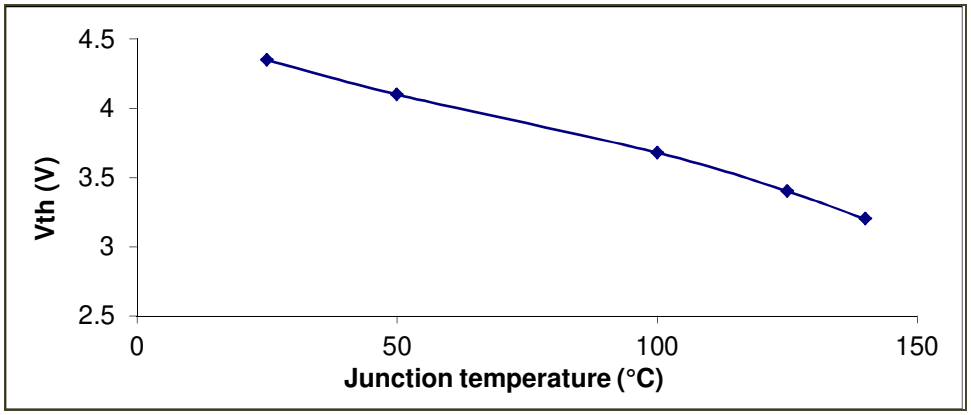

Fig.14. The measured threshold voltage for the IGBT IRGBC20U as a function of temperature

From figure 14, the threshold voltage of the IGBT as a function of junction temperature value can be approximated by a simplified linear equation as:

$V_{th} = -0.009 * T_j + 4.6$ (11)

*V.2.3. Voltage Rise Time (t_{rv}) :*In this section, we try to improve the influence of temperature and forward current I_F on the the$(dV/dt)_{off}$ capability at the turn-off behavior of IGBT. Figure 15illustrates the evolution of the collector-emitter voltage $V_{CE}(dV/dt)$ during the turn-off transition of the IGBT (IRGBC20U) versus the junction temperature Tj. When increasing temperature, the P-base resistance will also increase, because of a reduction in carrier mobility. This, cause a reduction in $(dV/dt)_{off}$ capability [17].

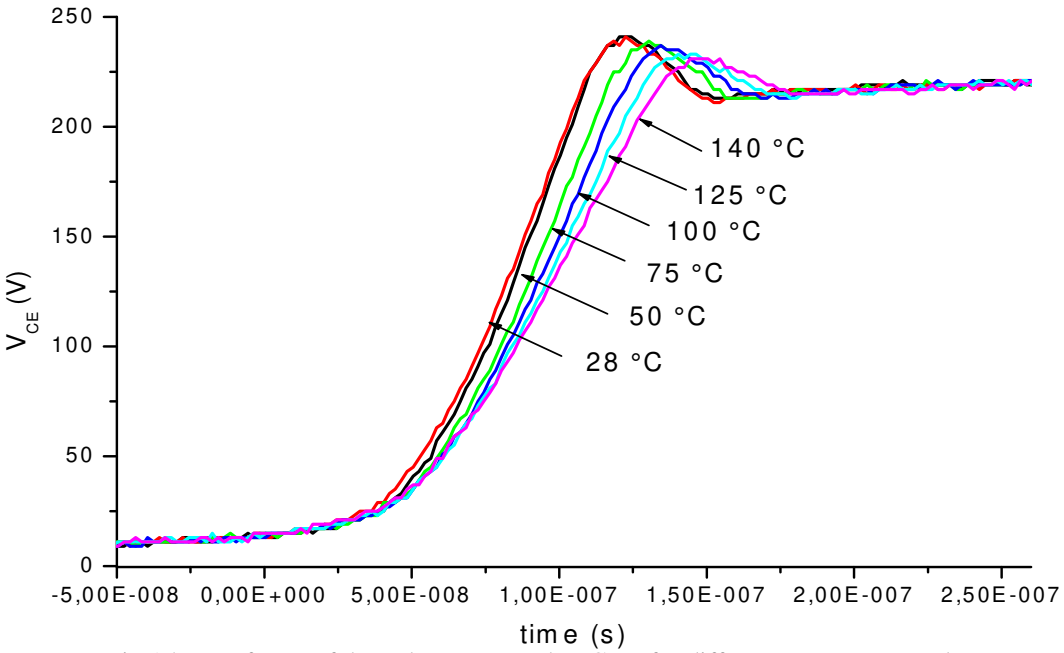

Fig.15.Waveforms of the voltage across the IGBT for different temperature values

Fig.16 shows the variation of the $(dV/dt)_{off}$ of the IGBT (IRGBC20U) versus the junction temperature under different load currents. The $(dV/dt)_{off}$ of the collector-emitter voltage varies with the amount of load current in a way similar to loading a capacitor by a constant current.

The variation of the voltage rise time (t_{rv}) as a function of load current and junction temperature is given by:

$$t_{rv} = \frac{I_F}{\frac{dV}{dt}_{off}(T_j, I_F)}$$

In practice, a fixed gate resistor is used and the variation of the slope rate of the voltage is the only function of the current magnitude and junction temperature.

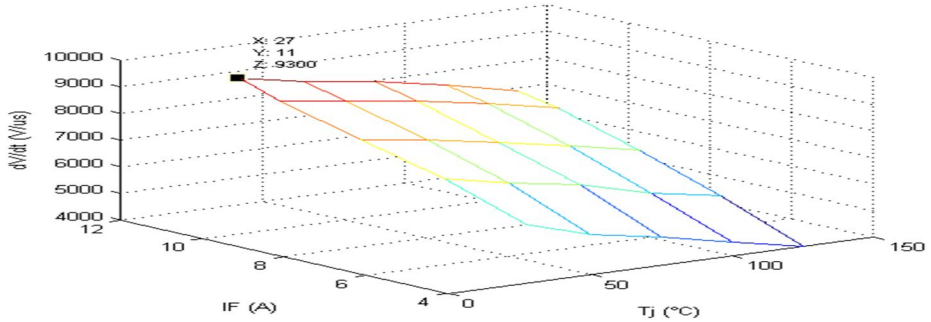

Fig.16.Variation of $(dV/dt)_{off}$ of the IGBT (IRGBC20U) versus the current magnitude $I_F$and the junction temperature Tj.

*V.2.4. Current full time(t_{fi}) and tail current time (t_{tail}) :*The switching losses during turn-off of an IGBT are highly influenced by the dynamic behavior of the collector current. First, the current fall time characterizes the transition from off-state to on-state. Second, bipolar devices like IGBT suffer from the so-called "current tail", which results from slow recombination and removal of carriers during turn-off and causes significant losses.

Figure 17 shows the waveforms of the collector current during the turn-off transition of the IGBT (IRGBC20U) versus the junction temperature T_j. We remark that the lifetime will increase as increasing temperature, and this will result in a larger current tail which increases the switching turn-off losses.

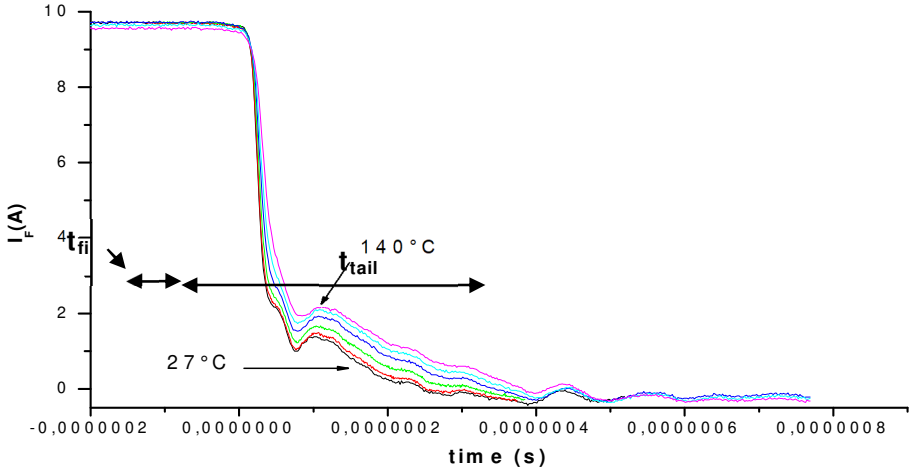

Fig.17. Influence of junction temperature on the evolution of the current flowing through the IGBT during turn off switching

Figure 18 illustrate the variation of the residual IGBT storage charge Q_{tail} versus the magnitude current I_F and the junction temperature Tj.

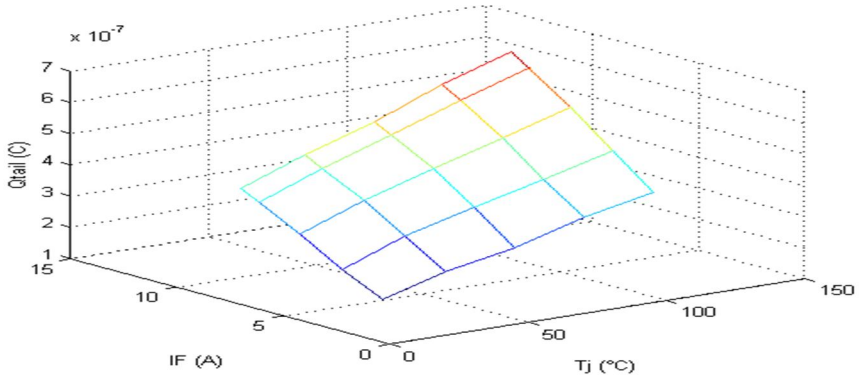

Fig.18. Evolution of the Q_{tail} (IRGBC20U) according to the magnitude current I_F and the junction temperature Tj

In fact, based on experimentations we have deduced the evolution of the fall time (t_{fi}) and the tail current time (t_{tail}) of the IRGBC20U as a function of load current and junction temperature.

VI. VALIDATION OF THE EXTRACTED PARAMETERS FOR SABER ELECTROTHERMAL MODELS

To validate the developed electrothermal average model, we will use as references the electro-thermal models of semiconductor components developed in the SABER simulator.

The electrothermal model for the IGBT has been developed by Hefner and is a standard library part in the SABER® circuit simulator. The electro-thermal diode model also is a standard library component and is based on the unified diode model developed in [18-19].

Figure 19 shows the electrothermal model for the IGBT, for example, and the corresponding electrical and thermal terminals. The electrical model calculates power dissipation, which is used by the 1D thermal model to evaluate the temperatures. Temperatures in return influence the electrical parameters, thus requiring a two-way coupling.

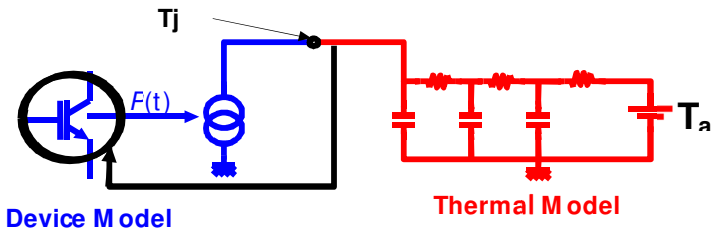

In SABER simulator the devices model parameters are extracted using an advanced parameter extraction sequences [20-21].

Table 2 and 3 show the list of the extracted parameters for the IGBT and diode.

Table 2. IGBT Electrothermal parameters

Parameters	Value
A (cm^2)	0,11
A_{gd}(cm^2)	0,033
W_L (µm)	58
W_H (µm)	14,5
V_{th} (V)	4 ,5
V_{td} (V)	-4 ,5
K_{plin0} (A /V2)	1,1
K_{psat0} (A /V2)	0,9
C_{gs}(nF)	0,24
C_{ox}(nF)	0,4
N_L (cm^{-3})	1,3*104
N_H (cm^{-3})	2 *1017
τ_H (µs)	0,25
τ_L(µs)	0,1
1/θ (V)	70
I_{sne} (10^{-14} A)	8
τ_{H1}(-)	1.4
V_{t1}(mV/K)	-0.011
I_{sne1}(-)	1.1
K_{plin1}(-)	1.0286
K_{psat1}(-)	2.1032

Table 3.Diode Electrothermal parameters

Parameters	Value
ISL(A)	6*10-5
NL(-)	1.4
BV(V)	600
CJO(F)	1nF
Tsw(s)	10n
TT(s)	16n
XTI(-)	-2.36
TNL1(-)	-8.75*10-4
TNL2(-)	-6.54*10-6
BETA(-)	1.8
BEATSW(-)	1*10-6

1) Validation of static Characteristics: Figure 20 shows the static characteristics of both the measured and simulated IGBT characteristics.

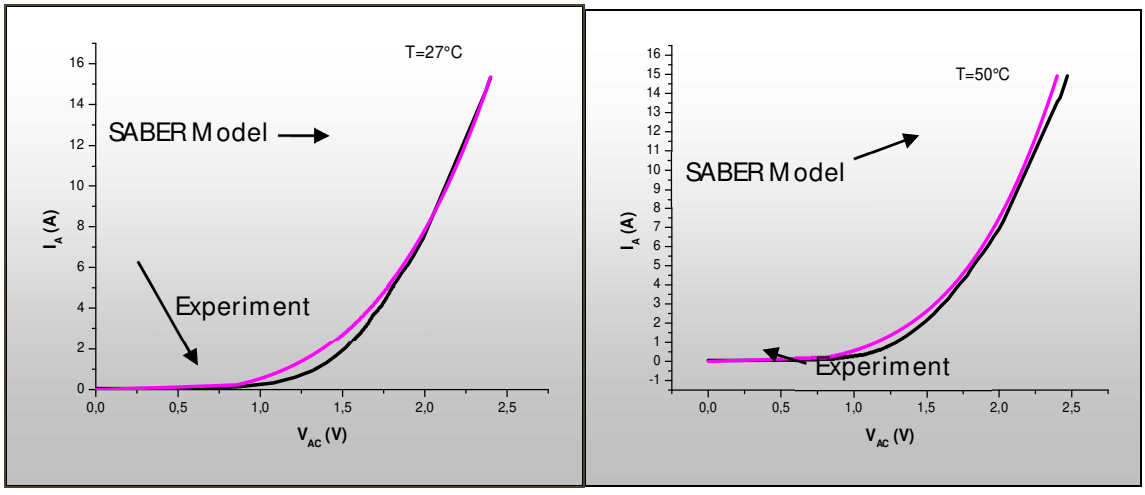

Fig.20. The forward I-V curves given by experimental and simulation ways (25 and 50 °C)

Figure 21 shows the forward characteristics of both the measured and simulated diode characteristics. The measured data is shown in continuous line and the simulated result is shown in the dotted line in the following figures.

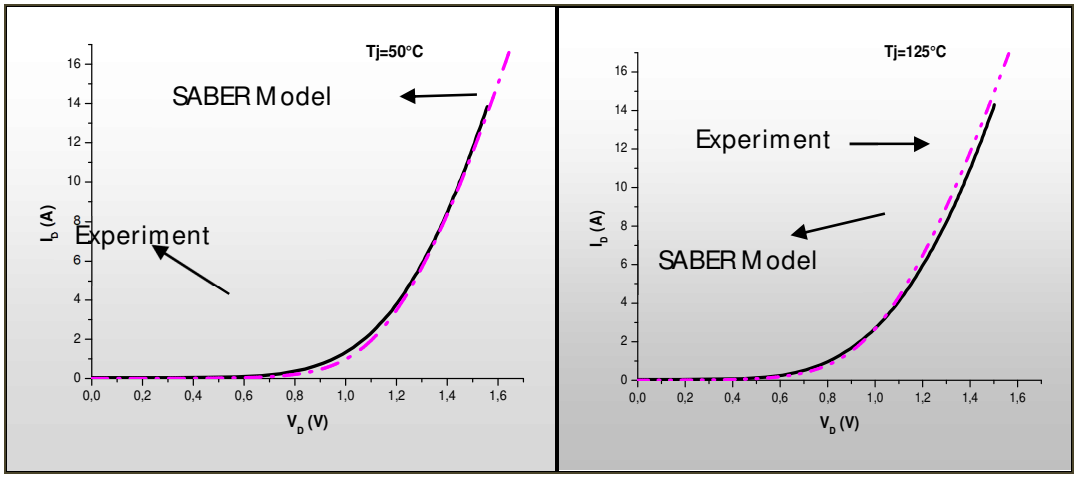

Fig.21. Forward I-V curves given by experimental and simulation ways of the diode BYT12P600

A good agreement isobserved between the physics-basedmodel prediction and the experimentation.

B. Validation of Dynamic Characteristics

VI.2.1 Diode device: In order to validate the accuracy of the diode model in SABER simulator, experiments are done on the diode during reverse recovery phenomena. Figure 22 shows the good agreement between experimental waveforms and the used model results. In fact diode models implemented in SABER will be used to validate the developed non ideal averaged model.
As it's shown in figure 22 the diode electrothermal model suit well with real electrothermal behavior of this diode.

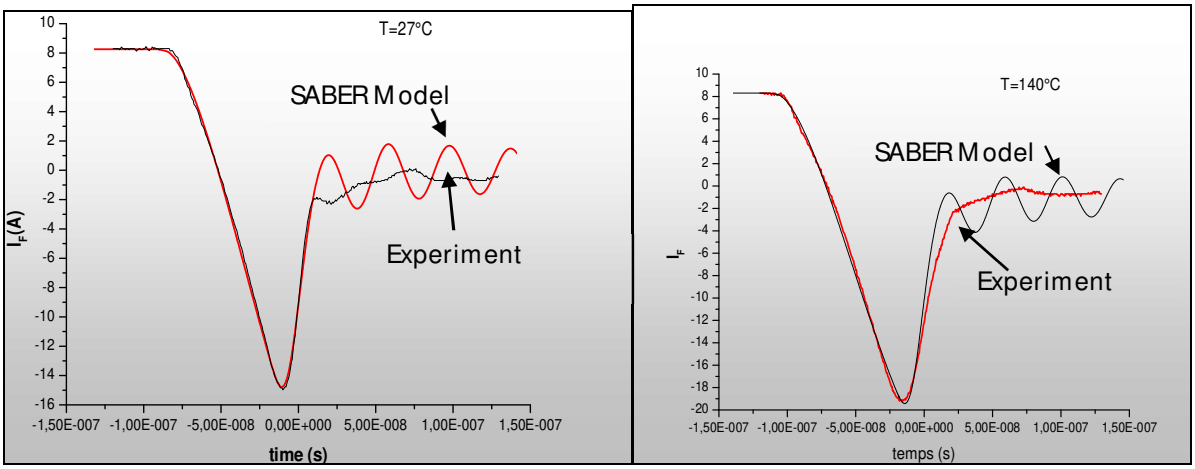

Fig.22. dynamic behavior of the electrical waveforms on the "BYT12P600" diode obtained by SABER electrothermal models and experiment. (V_R=200V and forward current I_F=8A)

VI.2.2 IGBT device: In order to estimate accurately losses value (during on and off switching time) in the IGBT, the electrical parameters of the IGBT model are expressed as function of the junction temperature of the device. Figure 23.a shows the evolution of the estimated energy losses during turn on phases (E_{on}) as a function of junction temperatures obtained by experiments and SABER model. Figure 23.b shows the E_{on} as a function of load current obtained by SABER model and experiments.

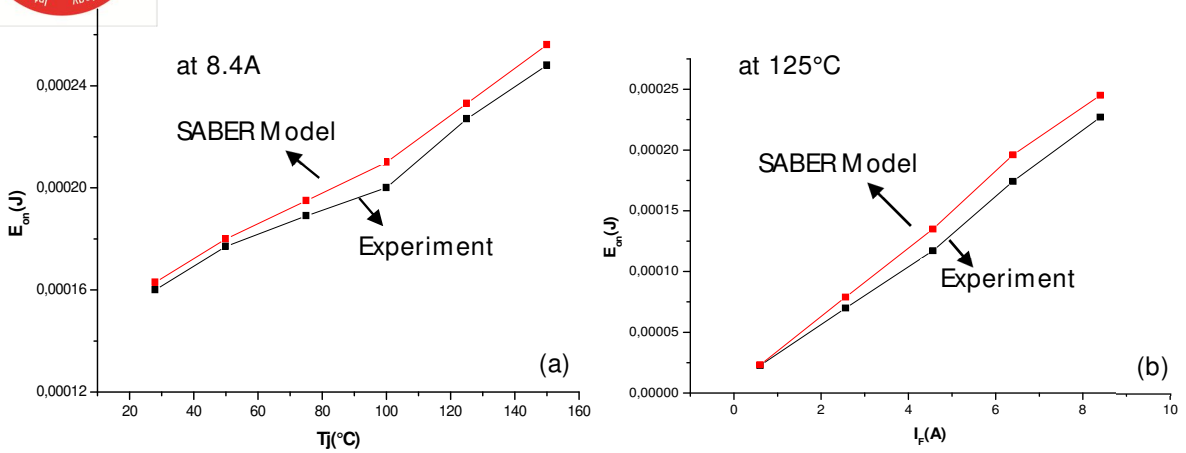

Fig.23. IGBT turn-on energyE_{on} versus (a) junction temperature and (b) forward current

Figure 24.a and Figure 24.b show the same study for turn off energy (E_{off}).

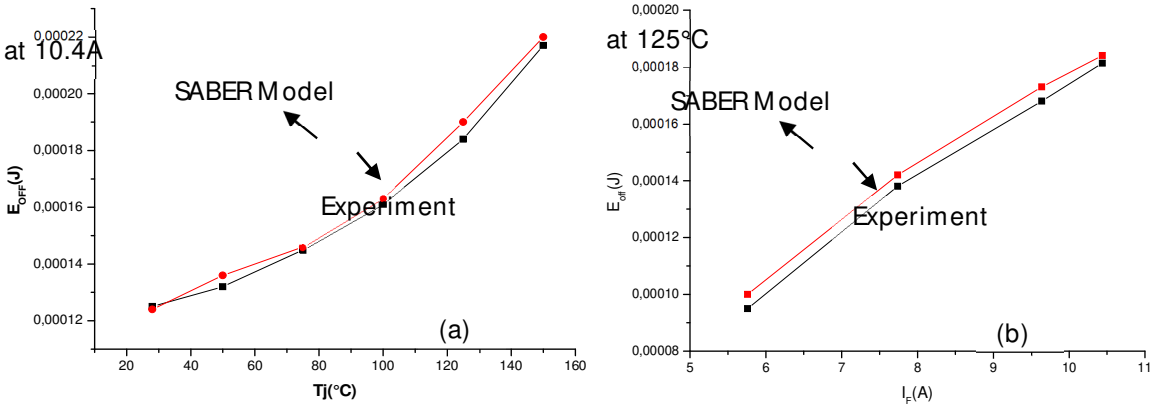

Fig.24. IGBT turn-off energy E_{off} versus (a) junction temperature and (b) forward current

These results shows the good accuracy of the electrothermal model implemented in SABER simulator.

VII. APPLICATION OF THE PROPOSED ADVANCED MODEL

In order to validate the developed electrothermal average model (Model 1) accuracy, SABER simulations are performed in the case of DC-DC and DC-AC converters. The simulation results obtained by SABER are considered as a reference. Also, to show theperformanceof the developed electrothermal average model, we compared its results with a pure electrical average model(Model2) [11].

The switching cell is composed of an IGBT (IRGBC20U) and a diode (BYT12P600).

A. The DC/DC converter (N-cell)

The validation of the proposed averaged model is performed using a BUCK converter shown in Figure 25. The ambient temperature was assumed to be equal to 27°C during simulations.

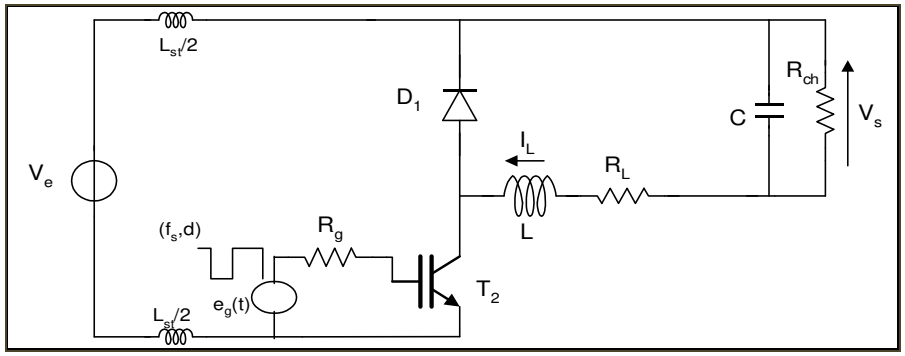

Fig.25. The used buck converter circuit

The different circuit parameter values are listed in Table 4:

TABLE 4
ELECTRICAL AND THERMAL PARAMETERS OF THE SELECTED BUCK CONVERTER

Parameter	Description	Value
V_e	Input voltage	200 V
eg	Gate drive voltage	15 V
L	Inductance	1200µH
C	Capacitance	470µF
R_L	Inductor esr	0.1Ω
R_{ch}	Load resistance	25Ω-10Ω - 14Ω
R_g	Gate drive resistance	68Ω
fs	Switching frequency	10KHz
L_{st}	DC loop inductance	100nH
R_{th_d}	Thermal resistance of the heat sink (diode)	0.2°C/W
R_{th_M}	Thermal resistance of the heatsink(MOSFET)	0.2 °C/W

During surge current conditions, junction temperature in the semiconducteur devices increases and electric phenomena in these devices can be highly affected. In fact, figure 26 shows the evolutions of the averaged dissipated power in the IGBT during a surge phase. We can see the good agreement between the developed electrothermal averaged model (model 1) waveforms and the SABER electrothermal model results which are considered as a reference.

When only electrical phenomena are taken into account in the classical averaged model (model 2) the estimated dissipated power in the IGBT is very less than the real dissipated power. An imported error is registered between the classical averaged model and the proposed electrothermal averaged model.

Figure 27 shows the evolution of the junction temperature in the IGBT during the serge conditions obtained by the three models. It is shown that a simplified one-direction coupling between the electrical and thermal model is not sufficient to estimate accurately the power converter behavior.

The simulation of 4s of converter electrical evolution was carried out during 1H30min with SBER simulator. Using the proposed electrothermal averaged model, the obtained simulation time cost is equal to 2min with the same processor performance. The improvement in simulation cost is about 45 in favor of the electrothermal averaged model.

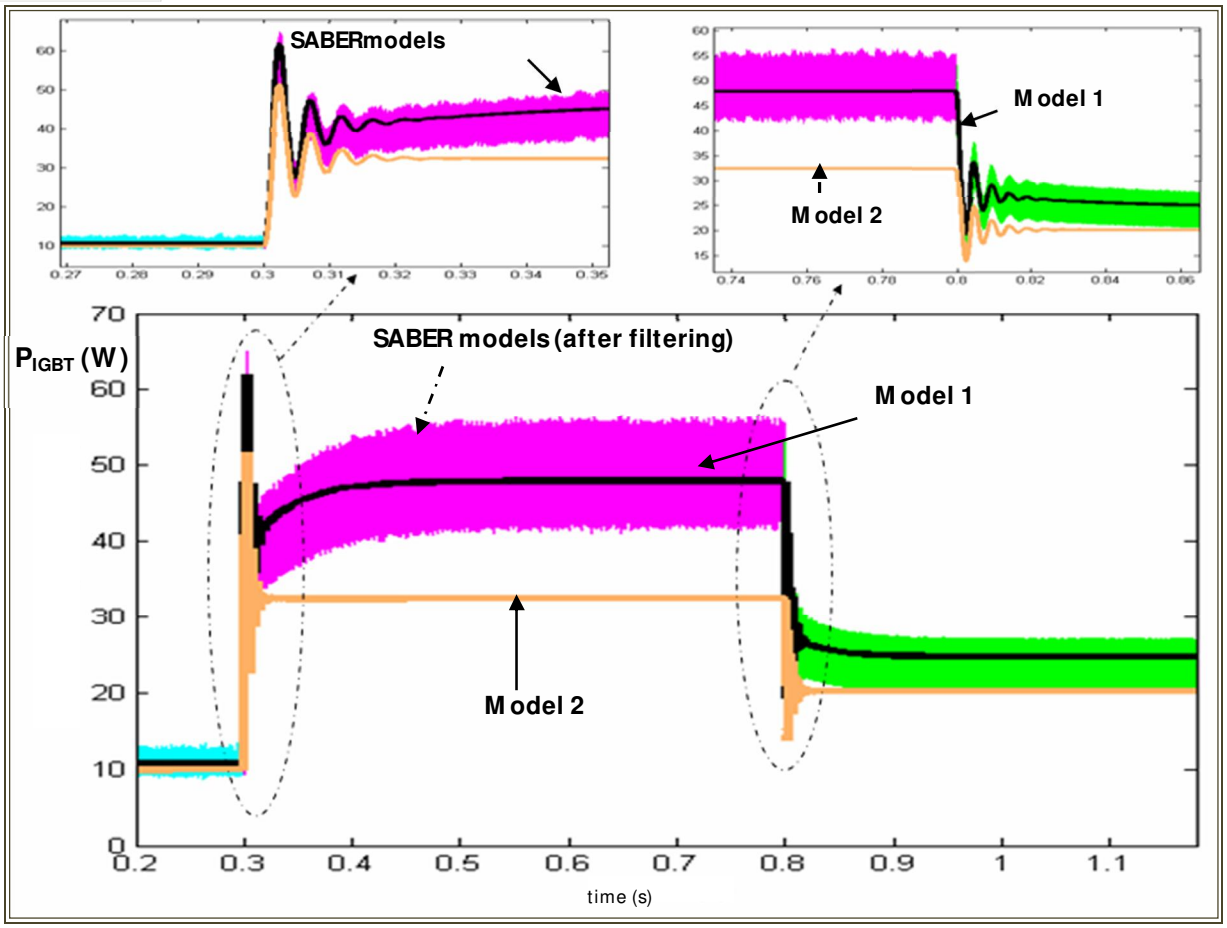

Fig.26. The evolution of the average dissipated power in the IGBT obtained with the developed electrothermal averaged model (model 1), the electrical averaged model (model 2) and SABER model after filtering

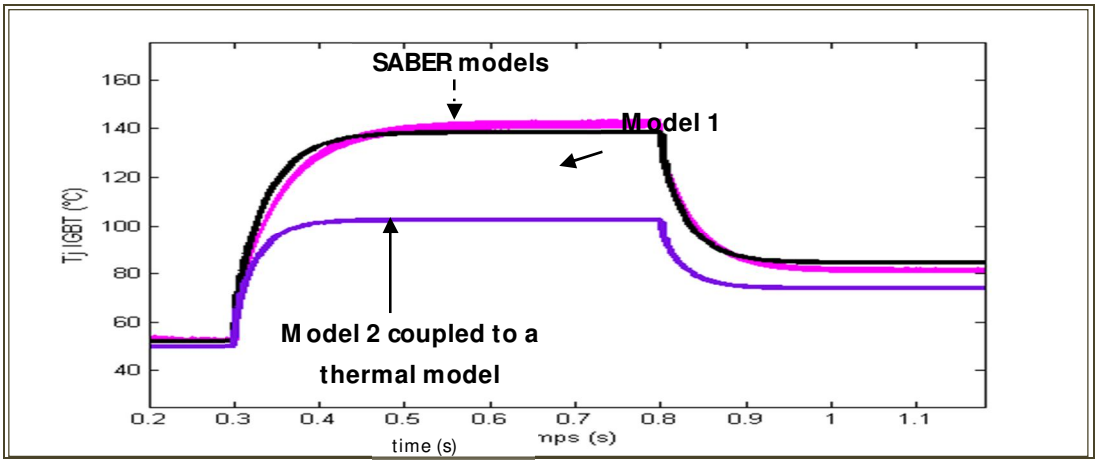

Fig.27. The evolution of the IGBT junction temperature obtained with the developed electrothermal averaged model(model 1), the pure electrical averaged model (model 2) coupled to a thermal model and SABER model

B. The DC/AC converter (Ncell, P-cell)

To validated the electrothermal behavior of the developed averaged model a bidirectional PWM-Switch is used in an inverter as shown in figure 28.

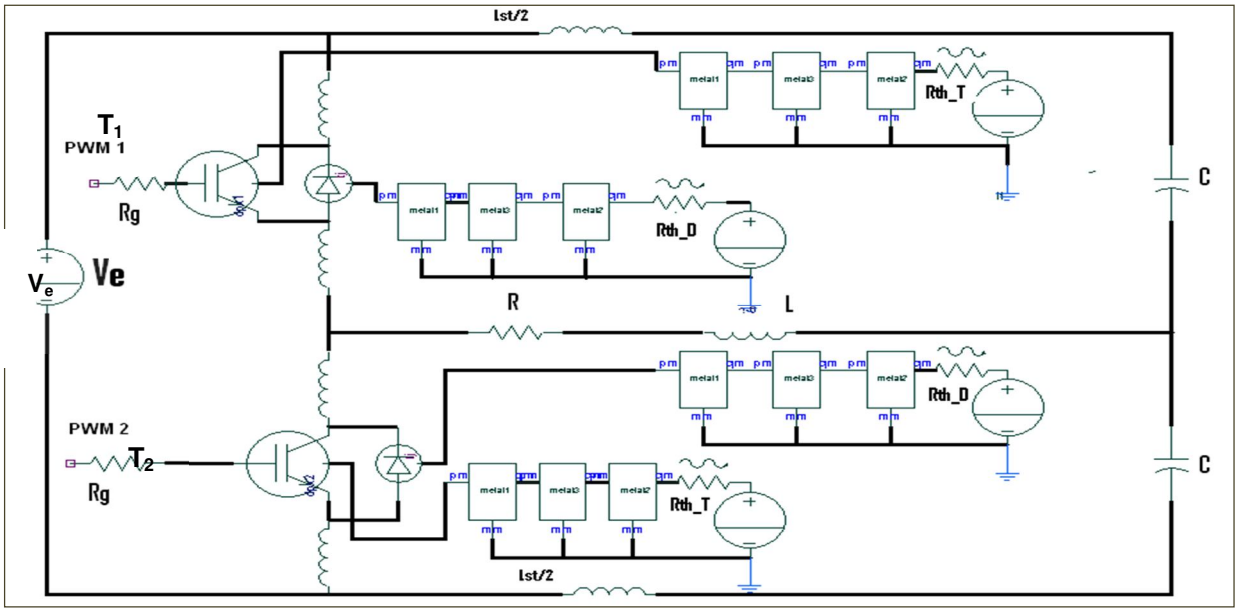

Fig.28. The electrical circuit of the studied DC-AC converter including devices electrothermal models

The different circuit parameter values are listed in Table 5:

TABLE 5
ELECTRICAL AND THERMAL PARAMETERS OF THE SELECTED DC/AC CONVERTER

Parameter	Description	Value
V_e	Input voltage	200 V
eg	Gate drive voltage	15 V
L	Inductance	5mH
C	Capacitance	2200µF
R_{ch}	Load resistance	8Ω
R_g	Gate drive resistance	68Ω
Fs	Switching frequency	10KHz
L_{st}	DC loop inductance	100nH
R_{th_d}	Thermal resistance of the heat sink (diode)	10°C/W
R_{th_M}	Thermal resistance of the heatsink(IGBT)	12 °C/W

Figure 29 and 30 shows the evolution of the dissipated power and the estimated junction temperature in the IGBT respectively. These results are obtained with the refined model(SABER), the classical electrical averaged model, and the developed electrothermal model. The obtained waveforms show a good agreement between the proposed electrothermal averaged model and the refined model. An important error is registered when a classical electrical averaged (model 2) model is used.

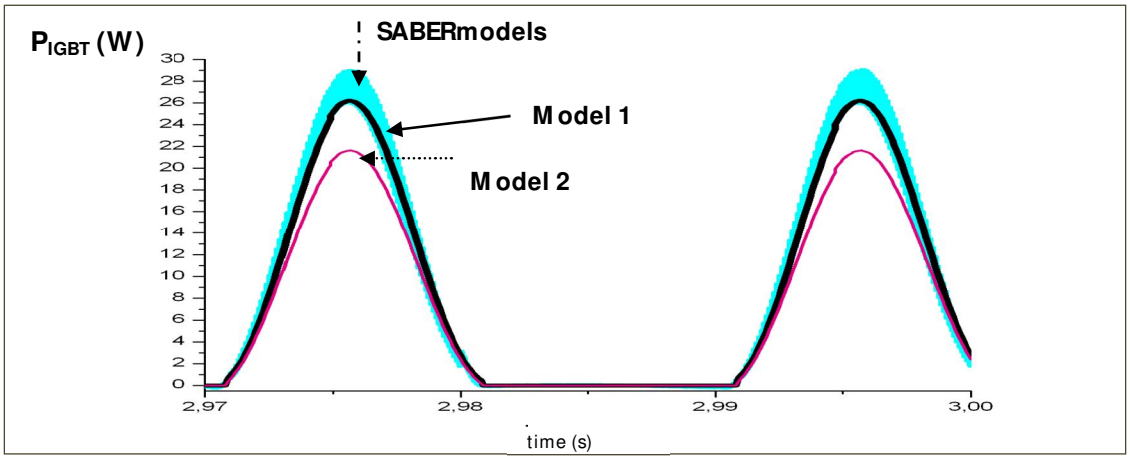

Fig.29. The evolution of the average dissipated power in the IGBT obtained with the developed electrothermal averaged model (model 1), the electrical averaged model (model 2),and SABER model after filtering

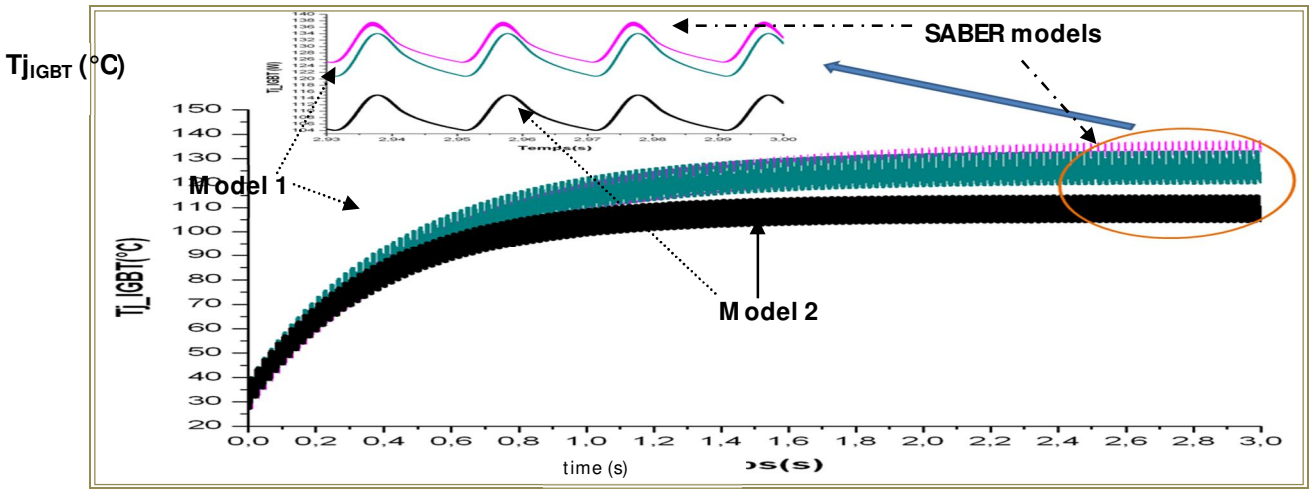

Fig.30. The evolution of the IGBT junction temperature obtained with the developed electrothermal averaged model (model 1), the electrical averaged model (model 2) coupled to a thermal model and SABER model

VIII. CONCLUSION

In this paper we have developed an advanced PWM-Switch electrothermal averaged model. Contrarily to the classical averaged model, the proposed model takes into account the device non-linearity (on state voltage and switching characteristics), the circuit stray inductance, the driving signals nonlinearity (dead times), and the junction temperature evolution. The device's non-linearity can be evaluated from the manufacturer data sheets or by experimental tests on the studied devices. The obtained average model corresponds directly to the original converter circuit. Only the switches are replaced by their average models.

Taking into account the device's switching parameters and their variations according to the temperature, the proposed averaged model, allows an accurate estimation of the total dissipated power in the semiconductor devices.

The proposed electro-thermal model gives a good trade-off between accuracy, efficiency, and CPU-cost. It can be implemented in any circuit-oriented simulation tool.

REFERENCES

[1] Zhen Hu,Wenfeng Zhang, Juai Wu, "An Improved Electro-Thermal Model to Estimate the Junction Temperature of IGBT Module" *Electronics* **2019**, *8*(10), 1066, 20 September 2019

[2] Kati Sidwall, Paul Forsyth, "A Review of Recent Best Practices in the Development of Real-Time Power System Simulators from a Simulator Manufacturer's Perspective"

[3] Ceccarelli, Lorenzo; Bahman, Amir Sajjad; Iannuzzo, Francesco; Blaabjerg, Frede, "A Fast Electro-Thermal Co-Simulation Modeling Approach for SiC Power MOSFETs" Proceedings of the 2017 IEEE Applied Power Electronics Conference and Exposition (APEC)

[4] F. Blaabjerg, K. Ma and D. Zhou, "Power electronics and reliability in renewable energy systems", IEEE International Symposium on Industrial Electronics (ISIE), July 2012, pp. 19-30.
[5] Nicolae-Cristian Sintamarean, FredeBlaabjerg, "Real Field Mission Profile Oriented Designof a SiC-Based PV-Inverter Application"IEEE TRANSACTIONS ON INDUSTRY APPLICATIONS, VOL. 50, NO. 6, NOVEMBER/DECEMBER 2014
[6] Kojima T, Yamada Y, Ciappa M, Chiavarini M, Fichtner W. A novel electro-thermal simulation approach of power IGBT modules for automotive traction applications. Proceedings of 2004 International Symposium on Power Semiconductor Devices & ICs, Kitakyushu, 2004.
[7] Mantooth HA, Hefner AR. Electro thermal simulation of an IGBT PWM inverter. IEEE Transaction on Power Electronics 1997; 12(3):474–484.
[8] Hefner R, Blackburn DL. Thermal component models for electro-thermal network simulation. IEEE Transactions on Components Package Manufacture Technology 1994; 17:413.
[9] Laprade A, Randal RH. Numerical method for evaluating IGBT losses. Application Note 7520 Rev. A1.
[10] A.AMMOUS et al, An advanced PWM-Switch Model including semiconductor device nonlinearities, IEEE Transactions on Power Electronics. Vol. 18, No.5, September 2003, pp.1230-1237
[11] S.ABID et al, Advanced Averaged Model of PWM-Switch operating in CCM and DCM conduction modes, IREE. Vol. 2, No.4, August 2007, pp.544-556
[12] Edwin Van Dijk et all, PWM-Switch Modeling of DC-DC Converters, IEEE Transactions on Power Electronics, Vol. 10, No. 6, November 1995, pp. 659-664.
[13] Fang Z. Peng et all, "Power Electronics' Circuit Topology – the Basic Switching Cells" Proceedings of 2005 PESEC
[14] A. Ammous et all, " Choosing a thermal model for electrothermal simulation of power semiconductor Devices" IEEE Tran. On Power Electronics, Vol 14, No 2, Mars 1999.
[15] A.AMMOUS et all, Developing an equivalent thermal model for discrete semiconductor packages, Elsevier International Journal of thermal sciences 2003 pp533-539
[16] FredeBlaabjerg and John K.Pedersen, Optimized Design of a Complete Three-Phase PWM-VS Inverter, IEEE Transactions On Power Electronics, Vol 12, No 3, MAY 1997
[17] J. Baliga, "Modern Power Devices", New York: John Wiley and sons, 1987
[18] H. Mantooth, J. Duliere, "A unified diode model for circuit simulation," IEEETrans. on Power Electronics, vol. 12, no. 5, Sept. 1997.
[19] A.R. Hefner, "A Dynamic Electro-Thermal Model for the IGBT," IEEE Trans. On Industry Applications. vol. 30, p. 394, 1994.
[20] Jose Miguel Ortiz-Rodriguez, "Electro-Thermal Modeling of a Power Electronic Module," University of Puerto Rico Maya Guez Campus, Master of Science Thesis, 2004.
[21] Gary E. Dashney, "Basic semiconductor thermal measurement," Motorola Semiconductor products sector, Phoenix, Arizona, Application note AN1570.

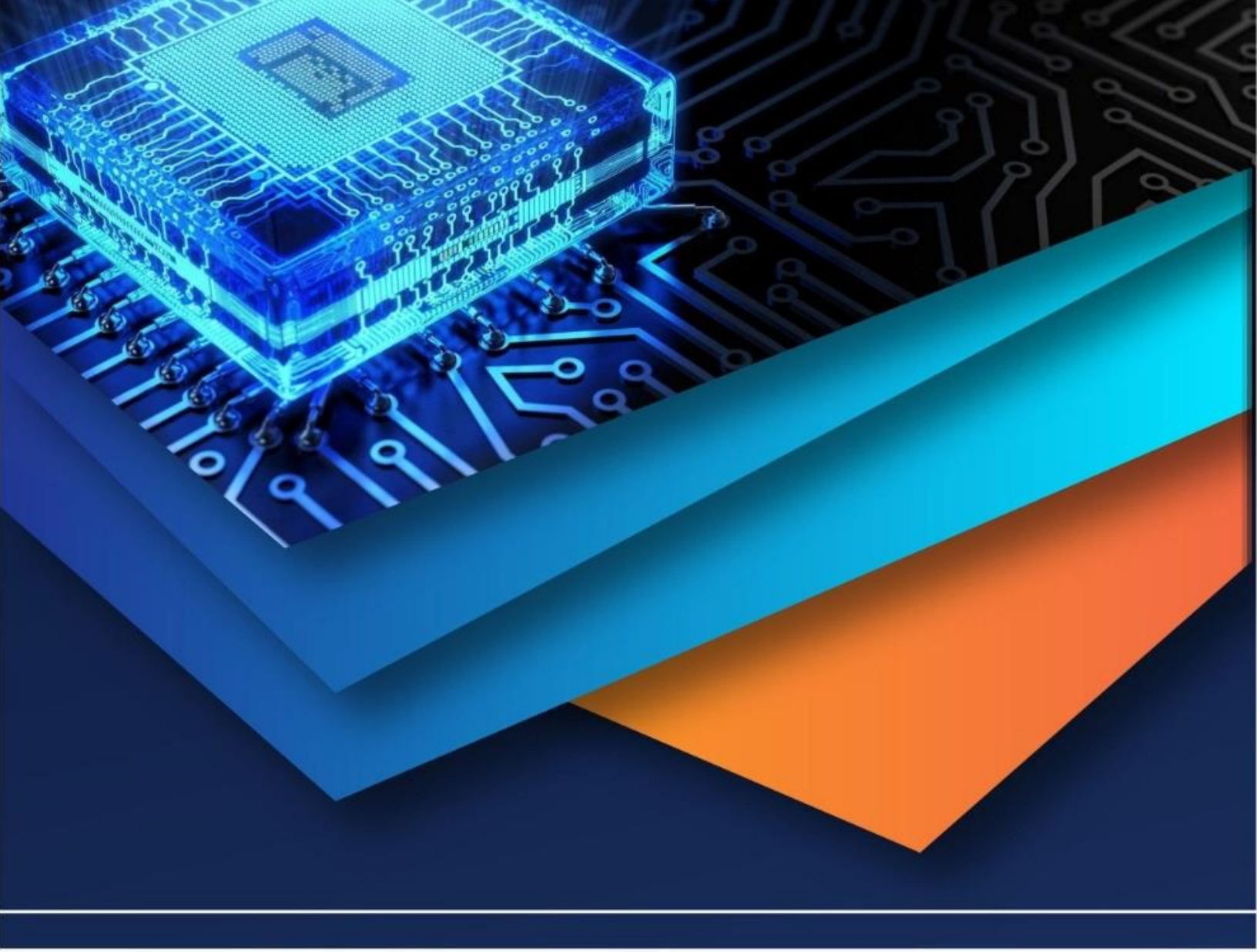

10.22214/IJRASET

45.98

IMPACT FACTOR: 7.129

IMPACT FACTOR: 7.429

INTERNATIONAL JOURNAL FOR RESEARCH

IN APPLIED SCIENCE & ENGINEERING TECHNOLOGY